

Dalton Transactions

Accepted Manuscript



This is an *Accepted Manuscript*, which has been through the Royal Society of Chemistry peer review process and has been accepted for publication.

Accepted Manuscripts are published online shortly after acceptance, before technical editing, formatting and proof reading. Using this free service, authors can make their results available to the community, in citable form, before we publish the edited article. We will replace this *Accepted Manuscript* with the edited and formatted *Advance Article* as soon as it is available.

You can find more information about *Accepted Manuscripts* in the [Information for Authors](#).

Please note that technical editing may introduce minor changes to the text and/or graphics, which may alter content. The journal's standard [Terms & Conditions](#) and the [Ethical guidelines](#) still apply. In no event shall the Royal Society of Chemistry be held responsible for any errors or omissions in this *Accepted Manuscript* or any consequences arising from the use of any information it contains.

Nickel(II) complexes with flexible piperazinyl moiety : studies on DNA and protein binding and catecholase like properties

Mriganka Das, RajendarNasani, ManideepaSaha, Shaikh M Mobin, SumanMukhopadhyay*

Department of Chemistry, School of Basic Sciences, Indian Institute of Technology Indore, IET-DAVV Campus, Khandwa Road, Indore 452017, India. Tel : +91 731 2438 705 Fax: +91 731 2361 482 E-mail: suman@iiti.ac.in

Abstract

Four new mononuclear Ni(II) complexes $[\text{Ni}(\text{L}^1)]\text{ClO}_4$ (**1a**), $[\text{Ni}(\text{L}^2)]\text{ClO}_4$ (**1b**), $[\text{Ni}(\text{SCN})_3(\text{CH}_3\text{OH})(\text{aminoethylpiperazineH})]$ (**2a**), and $[\text{Ni}(\text{DMSO})_4(\text{aminoethylpiperazineH})](\text{ClO}_4)_3$ (**2b**) have been synthesized from two Schiff base ligands [$\text{L}^1 = 1\text{-phenyl-3-}((2\text{-}(\text{piperidin-4-yl})\text{ethyl})\text{imino})\text{but-1-en-1-ol}$ and $\text{L}^2 = 4\text{-}((2\text{-}(\text{piperazin-1-yl})\text{ethyl})\text{imino})\text{pent-2-en-2-ol}$] by exploiting the flexibility of piperazinyl moiety. Structural analysis reveals that **1a** and **1b** are square planar complexes where piperazine rings are in boat conformations whereas hydrolysis of Schiff bases (L^1 and L^2) occurs during formation of octahedral complexes (**2a** and **2b**) where piperazine rings are in chair conformations. Screening tests was conducted to quantify the binding ability of complexes (**1a**, **1b** and **2a**) towards DNA, BSA and HSA and it has been found that square planar complexes (**1a** and **1b**) are showing more effective binding properties over octahedral complex (**2a**). Furthermore enzyme kinetic studies reflect that square planar complexes (**1a** and **1b**) are also effective in mimicking catecholase like activities over octahedral complex (**2a**). Among all the complexes **1a** was found to be the most promising molecule among these series due to its large binding affinity towards different biomacromolecules and higher T.O.N in catechol oxidation reaction.

Introduction

Use of transition metals by nature in different biological processes drive the quest of the scientist to understand the underlying principles of its functionality which eventually helps to develop different structural and more importantly functional model systems.¹⁻⁶ Apart from studying different biological processes induced by metal ions many new molecules have been also

developed over the years showing interesting properties like antibacterial, antifungal, antimicrobial and anticancer/antiproliferative activity where the transition metal ion performs a pivotal role in terms of structural organisation and overall functionality.⁷⁻¹¹ Furthermore interactions of small metal complexes with DNA and proteins are the key research areas of current years as there are enough potentials of development of new therapeutic agent particularly showing antitumor properties and possibility of the transportation of these molecules throughout the physiological system via protein binding.¹²⁻¹⁵ Among the various transition metal ions nickel has already shown promising activities in many of the above mentioned areas. Though many transition metal complexes so far have been tried and screened as a potential pharmaceuticals, nickel complexes in medicinal biochemistry is comparatively rare. However, there few reports where nickel complexes have been screened for DNA binding along with DNA adduct formation, oxidative damage of DNA and DNA-DNA crosslink formation revealing the antitumor activity.¹⁶⁻²⁰ The amazing binding properties of serum albumin towards different endogenous and exogenous compounds provides the vital ability for this group of plasma protein to take an active role for possible drug delivery. Study of interaction of small molecules with different types of serum albumin is also crucial for the understanding of metallopharmaceutical pharmacokinetics and structure-activity relationship. However the nature of interaction between proteins and different nickel complexes which have been studied so far is limited in nature and requires more studies for generalization.²¹⁻²⁴

On the other hand di-nuclear nickel (II) centers have been also studied for the possible catechol oxidase like properties.²⁵⁻²⁸ Most of the researchers have focussed on di-nuclear nickel systems so far to match the original enzyme structurally where exist a dimeric-copper active center. There are only few reports where mononuclear nickel complexes have been studied for possible catecholase like activities.²⁹⁻³⁰ It has been also indicated in some cases that extra positive charge on ligand induces higher activity towards catechol oxidation.²⁹⁻³⁰

Herein, we report the synthesis and characterization of four new mononuclear nickel complexes
 $[\text{Ni}(\text{L}^1)]\text{ClO}_4$ **1a** $[\text{HL}^1 = 1\text{-Phenyl-3-(2-piperazin-1-yl-ethylimino)-but-1-en-1-ol}]$,
 $[\text{Ni}(\text{L}^2)]\text{ClO}_4$ **1b** $[\text{HL}^2 = 4\text{-}((2\text{-(piperazin-1-yl)ethyl)imino)pent-2-en-2-ol}]$
 $[\text{Ni}(\text{SCN})_3(\text{CH}_3\text{OH})(\text{aminoethylpiperazineH})]$ **2a** and
 $[\text{Ni}(\text{DMSO})_4(\text{aminoethylpiperazineH})(\text{ClO}_4)_3]$ **2b**. The interaction of complexes **1a** and **1b** with DNA, BSA and HSA have been also studied which are showing promising results with very high

affinity towards DNA and albumin proteins. Moreover, **1a** and **1b** were also investigated for possible catechol like activity and particularly **1a** has shown very high activity towards the catalytic oxidation of 3,5-di-tert-butylcatechol (3,5-DTBC).

Results and discussions

Syntheses of the Complexes: The reaction of 1-Phenyl-1,3-butanedione/ acetyl acetone with amino ethyl piperazine in 1:1 molar ratio in chloroform led to the formation of Schiff base ligand HL¹ and HL² respectively (scheme 1). Though the ligand HL² was reported previously³¹ however ligand HL¹ is getting reported here for the first time. Upon reaction of L¹ and L² with nickel perchlorate in methanol a red colour solution was obtained which upon further concentration and layering with diethyl ether furnished red needle shaped compounds [Ni(L¹)]ClO₄ (**1a**) and [Ni(L²)]ClO₄ (**1b**), respectively (scheme 1). However, a similar procedure like synthesis of **1a** and further addition of ammonium thiocyanate in the reaction mixture induces hydrolysis of the Schiff-base and furnished [Ni(SCN)₃(CH₃OH)(aminoethylpiperazineH)] (**2a**) (scheme 1). Occurrence of such type of hydrolysis are also reported elsewhere.³² A similar method which has been followed for **1b** in water as solvent instead of methanol furnished a green coloured solution (possibly formation of an octahedral nickel complex)³³ and it was almost evaporated to dryness to obtain a green coloured powder. Upon dissolution of this green compound in DMSO (only solvent in which the green compound gets dissolved) and subsequent layering with methanol produced green coloured crystals of [Ni(DMSO)₄(aminoethylpiperazineH)](ClO₄)₃ (**2b**) (scheme 1). In this case also similar hydrolysis of the Schiff-base moiety has been observed. Both the ligands HL¹ and HL² have been characterized by ¹H and ¹³C NMR and ESI-MS spectroscopy. The new ligand HL¹ has shown all the characteristic peaks in ¹H NMR. The molecular peak was observed at 274.18 in ESI-MS spectrum(

S1). All the complexes have been characterized by IR and ESI-MS spectroscopy (except **2b** because of poor solubility), elemental analyses and singly crystal X-ray crystallography. IR spectra of complexes **1a** and **1b** have a prominent band around 1600 cm⁻¹ assignable to ν(C=N) stretching mode.³⁴ Moreover complexes **1a**, **1b** and **2a** show medium intensity band in the range of 3240-3305 cm⁻¹ due to ν(N-H) stretching.³⁴ However, for compound **2b** ν(N-H) stretching band is not visible because of the presence of relatively broad and stronger band centred around 3443 cm⁻¹ because of the presence of DMSO molecule in the complex.³⁵ In addition compound **1a**, **1b** and **2b** show very strong band around 1100 cm⁻¹ characteristics of presence of perchlorate

counterion.³⁴ For compound **2a** two well resolved bands for thiocyanate have been observed at 2118 and 2092 cm^{-1} , respectively.³⁴ The ESI-Mass spectra of compound **1a** and **1b** show the molecular ion peak at 330 and 268, respectively (fig S2 and fig S3). In case of **2a** the peak corresponding to $[\text{Ni}(\text{SCN})(2\text{-Piperazin-1-yl-ethylamine})]^+$ was observed at 245 (fig S4). Complex **2b** cannot be characterized by ESI-Mass spectroscopy because of low solubility of the compound.

Structure Description of the Complexes (1a) and (1b): These two structures are monomeric in nature and with square planar environment surrounding the nickel ions. The ligands are acting in tetradentate fashion with three N and one O atom completing the square base (fig 1). In both the complexes the bond lengths between Ni atom and N/O-donor centers are within the range of 1.8112(17) – 1.934(2) Å (Table 1), quite similar to those which have been reported earlier.³³ The average co-ordination bond angle around Ni center of square planar geometry is around 90° whereas least bond angle was observed for N(2)-Ni(1)-N(3) ($\sim 76^\circ$) (Table 1) due to the formation of chelated five membered ring piperazinyl moiety in boat conformation. In compound **1a** perchlorate ion was found to be disordered in nature. Furthermore, the independent molecules get connected with each other through hydrogen bonding viz. C8-H8A...O1 and C7-H7B...C16 to form a 1D chain (fig S5). Two such adjacent molecules are further joined by hydrogen bonding through perchlorate ion viz. C9-H9A...O111, C5-H5A...O111 and C16-H16...O333. Two such strands are additionally joined by the same interconnecting perchlorate ion via C6-H6B...O111 and C5-H5B...O222 (fig S6). This hydrogen bonded sheet structure in *bc*-plane is further extended along *a*-axis through C13-H13...O222 bonding to provide a 3D structure (fig S7). On the other hand in compound **1b** each counter perchlorate ion connects six different molecules through the following hydrogen bonding viz. C5-H5C...O333, N3-H3N...O333, C7-H7B...O333, C8-H8A...O333, C6-H6B...O111, C10-H10B...O444, C8-H8A...O222 and C7-H7A...O222 (fig S8), which ultimately leads to formation of a 3D network.

Structure Description of the Complexes (2a) and (2b): These two complexes are monomeric octahedral crystals of nickel ions which are crystallized in orthorhombic and monoclinic crystal systems, respectively. The two N donor atoms of amino ethyl piperazine fulfill the two coordination sites of octahedral geometry (fig 1). The piperzinyll ring takes the chair conformation where secondary nitrogen atom coordinates one extra proton and stays away from the coordination. The octahedral geometry surrounding the metal center is completed by three

coordinating thiocyanate ions getting attached to the nickel center via nitrogen atom and one methanol molecule which is coordinating in *trans* fashion with respect to tertiary nitrogen atom of amino ethyl piperazine. The protonated piperziny ring induced a hydrogen bonded 1D chain through N5-H5...S1 (fig S9) which is propagated along *a*-axis. Two such adjacent parallel chains are further joined by N5-H5...S3 and C5-H5B...S3 to form 2D hydrogen bonded network in *ab*-plane (fig S10). These 2D networks are further connected along the *c*-axis through O111-H101...S3 and N6-H2N...S2 to complete a 3D hydrogen bonded network (fig S11). The molecules are further joined by each other through hydrogen bonding to form a 3D hydrogen bonded network. In compound **2b** also the piperziny ring takes the chair conformation and act as bi-dentate ligand whereas the rest of the coordination positions are fulfilled by DMSO molecules (fig1). Three perchlorate counter ions are present in each molecule. The separated molecules are arranged in a linear fashion along *b*-axis directly through a distant hydrogen bonding viz. C5-H5B...C9. However there are eleven perchlorate ions observed surrounding a single molecule and connected through different hydrogen bonding; among them at least three perchlorate ions help to connect the adjacent molecules through hydrogen bonded network to maintain 1D chain. [C6-H6A...O555; N3-H...O666; C14-H14C...O222; C9-H9B...O222; C10-H10B...O444; N1-H2N...O777; C14-H14C...O222; C9-H9B...O444 and C10-H10B...O444] (fig S12). However, considering all the hydrogen bonding surrounding one particular molecule the structure is quite complex and it provides a 3D-polymeric hydrogen bonded network. In both the complexes the bond lengths between Ni atom and N/O-donor centers are within the range of 2.040(3) – 2.255(3) Å (Table 2), quite similar to those octahedral complexes which have been reported earlier.³³ All the hydrogen bonding parameters of all the complexes are compiled together in Table S1.

DNA binding studies between complexes and CT-DNA

As nickel complexes have a tendency to interact with DNA and proteins therefore we have performed various spectroscopic studies of nickel complexes (**1a**, **1b** and **2a**) with CT-DNA, BSA and HSA to understand the interaction of synthesized complexes on them. In complex **1a** two bands were observed in the high energy region at 340 and 250 nm, respectively. These bands are assigned as intra-ligand charge transfer band due to $n \rightarrow \pi^*$ and $\pi \rightarrow \pi^*$ transition. Any interaction with DNA is expected to perturb the intra-ligand centered spectral transitions. With the increase amount of CT-DNA it has been observed that for complex **1a** the $\pi \rightarrow \pi^*$ transition

is showing hyperchromism along with a slight red shift (fig S13A). This strong hyperchromic effect indicates considerable interaction of complex **1a** with CT-DNA. The DNA binding affinities of the complexes were compared by calculating the intrinsic binding constant K_b by following equation²³

$$\frac{[\text{DNA}]}{(\epsilon_a - \epsilon_f)} = \frac{[\text{DNA}]}{(\epsilon_b - \epsilon_f)} + \frac{1}{K_b(\epsilon_b - \epsilon_f)}$$

where [DNA] is the concentration of DNA in base-pairs, ϵ_a is the apparent extinction coefficient calculated by absorbance/ [complex], ϵ_f is the extinction coefficient of the complex in its free form, and ϵ_b is the extinction coefficient of the complex in the bound form. In both the cases when data was fitted in the above equation it gave a straight line with a slope of $1/(\epsilon_b - \epsilon_f)$ and an intercept of $1/K_b(\epsilon_b - \epsilon_f)$. The value of K_b was determined from the ratio of slope to intercept (fig S13B) which was found to be $4.5 \times 10^4 \text{ M}^{-1}$ which is on higher side as per different nickel complexes are reported so far.¹⁵ However for compound **1b** and **2a** we did not find any suitable CT band in the above mentioned region which can be monitored and therefore we have not performed any UV-vis study for these two compounds for DNA interaction.

To understand the interaction between complexes with CT DNA more clearly steady state competitive binding experiments using complexes **1a** and **1b** (complex **2a** did not respond in this study) as quenchers were undertaken where ethidium bromide (EB) was used as a fluorescent probe. EB is a planar cationic dye which emits intense strong fluorescent light in presence of DNA due to its strong intercalation between the adjacent DNA base pair. When complexes intercalate in DNA the probable binding sites for EB in DNA get decreased hence the fluorescent intensity of EB gets quenched. As the concentration of the nickel complexes increases, the reduction in the fluorescence intensity clearly indicates that the EB molecules are displaced from their DNA binding sites and are replaced by the metal complexes under investigation. The fluorescence quenching spectra of DNA bound EB by complexes **1a** and **1b** shown in (fig S14). Both the spectra is indicative of displacement of EB from CT-DNA as there are appreciable reduction in fluorescent intensity. However, this displacement is more prominent in **1a** than **1b**. Furthermore, K_q values for complexes **1a** and **1b** have been found to be 3.3×10^4 and $7.1 \times 10^2 \text{ M}^{-1}$, respectively which was obtained from classical Stern-Volmer equation.¹⁴ The binding constant (K_b) values obtained from the plot of $\log[(F_0-F)/F]$ vs $\log[Q]$ (from Scatchard equation)¹⁹(fig S15) were found to be 5.6×10^3 and $2.3 \times 10^3 \text{ M}^{-1}$ for complex **1a** and

1b respectively, reflecting more binding of complex **1a** with DNA to leach out more number of EB molecules originally bound to DNA than that of for complex **1b**.

Interaction of complexes with serum albumins by fluorescence quenching study:

Interaction of transition metal complexes with proteins are generally monitored by intrinsic fluorescence intensity. Binding of prospective molecules particularly to blood plasma protein are in center of attraction as the transport of drugs through the bloodstream is affected via the interaction of drugs with them.³⁶ To study the interaction of synthesized complexes with different proteins fluorescence quenching studies with BSA and HSA were carried out. The fluorescence property in BSA is mainly attributed due to the presence of three amino acids viz. tryptophan, tyrosine and phenyl alanine residues.³⁶ However, fluorescence quenching may happen because of several reasons like excited state reactions, ground state complex formation, energy transfer, molecular rearrangement and collision quenching. The fluorescence spectrum of **1a** with BSA indicates that there is a progressive decrease in the fluorescence intensity along with a significant red shift. The intensity of the fluorescent band observed at 340 nm was quenched to the extent of 15% of its initial intensity (fig 2). The shifting of the emission maxima towards lower energy indicates the probable energy transfer from the indole unit of the tryptophan to the protein bound compound. The fluorescence quenching data was further analyzed by the Stern–Volmer relation which again can be expressed in terms of bimolecular quenching rate constant and average life time of the fluorophore as shown in following equation³⁷

$$\frac{F_0}{F} = 1 + k_q\tau_0[Q] = 1 + K_{SV}[Q]$$

where F_0 and F are the fluorescence intensities in the absence and the presence of a quencher, k_q is the bimolecular quenching rate constant, τ_0 is the average life time of fluorophore in the absence of a quencher and $[Q]$ is the concentration of a quencher (Metal complexes). K_{SV} is the Stern–Volmer quenching constant in M^{-1} . However, in this case a plot with upward curvature concave towards y-axis was obtained. This positive deviation indicates a probable two way quenching by collision and as well as by complex formation with the same quencher. Moreover the value of k_q which shows normally the value in the range $10^{10} M^{-1}s^{-1}$ for dynamic quenching was found to be $7.7 \times 10^{12} M^{-1}s^{-1}$ indicating the role of static quenching in the present case.³⁸ The

value obtained for K_{SV} was 4.8×10^4 is also on higher side indicating a strong binding between BSA and **1a**.

The effect of addition of complex **1a** in HSA has a more dramatic effect on fluorescence quenching. The intensity of the fluorescent band decreased up to 5% of its initial intensity (fig 3). In Stern-Volmer plot at lower concentration of quencher **1a** it shows linearity however at higher concentration it shows quite high positive deviation from linearity. It indicates the formation of more than one ground state complex HSA-**1a** system, so it can be predicted that at lower concentration of **1a** the quenching could be started by a stable ground-state complex formation (1:1 type) however at higher concentration an upward bending in the direction of the F_0/F axis specifies the formation of the second (1:2 type) **1a**-HSA complex. Such 1:2 type complex formation for **1a**-HSA system may have stimulated due to the more flexible environment of HSA (than that of BSA) that have preferred to form some loose binding interaction of **1a** with HSA.³⁹

To determine the binding constant and number of binding site Scatchard equation was employed which is given by

$$\log \left[\frac{F_0 - F}{F} \right] = \log K_a + n \log [Q]$$

Where K_a and n are the binding constant and number of binding sites respectively, and F_0 and F are the fluorescence intensities in the absence and presence of the quencher respectively. Thus, a plot of $\log(F_0 - F)/F$ versus $\log[Q]$ (fig S16) can be used to determine the value of binding constant (from intercept) and number of binding sites (from slope). Calculation shows that the binding constant for **1a**-HSA is quite high $5.6 \times 10^9 \text{ M}^{-1}$ and the n value obtained was 2.12. The K_a and n value obtained for **1b**-BSA pair are 1.7×10^6 and 1.34 respectively which are also relatively on higher side with respect to other nickel complexes reported so far. All the relative data are compiled in table 3.

The interaction of complex **1b** with BSA and HSA in terms of fluorescence quenching is depicted in fig S17 and fig S18. The quenching of fluorescent band at 340 nm went up to 79% and 76% of their initial intensity for BSA and HSA, respectively. The K_a and n values obtained for these cases are found to be 4.9×10^3 , 5.1×10^3 , 1.07 and 1.03, respectively. It clearly indicates that the affinities of interaction of complex **1b** with different proteins are respectively weaker than complex **1a**. A probable reason for that can be envisaged as ligand L^1 will be less electron

donating than L^2 because of the presence of electron withdrawing phenyl group the relatively higher positive charge on metal-ion may induce more interaction with the donating site of the proteins in case of compound **1a** with respect to **1b**.

To get further insight regarding the type of quenching (static or dynamic) which is prevailing we have performed UV-vis absorption measurement of the protein with increasing concentration of the nickel complexes. Dynamic quenching generally only affects the excited state of the fluorophores and there are no changes observed in absorption spectra. However, formation of complex in ground state generally induces perturbation in the protein structure resulting a change in absorption spectrum of the fluorophore.²² In present case there is a considerable increase in the intensity of absorption for BSA and HSA respectively in the same wave length when they have been treated with complex **1a** separately with the gradual increase in the concentration of the nickel complex (fig S19A and S19B). This result indicates clearly that there is a formation of protein-**1a** complex in the ground state which is causing a change in the conformation of the protein and static quenching is contributing a major part in the total quenching of the fluorescence in the above mentioned study.²² A similar experiment with BSA and HSA when both of them have been treated with increasing concentration of complex **1b** revealed similar results (fig S20A and S20B). However the rate of decrease in absorption intensity is comparatively less and which reconfirms a weaker interaction of complex **1b** with the proteins with respect to complex **1a**.

Circular dichroism studies : To have a better understanding in nickel complex - protein binding mechanism and secondary structure changes of protein CD measurement was performed. (fig S21) shows the CD spectra of BSA along with BSA-**1a** and BSA-**1b** complex respectively. A negative CD band was observed with two characteristic bands at 208 and 222 nm which is indicative of negative cotton effect as a consequence $n \rightarrow \pi^*$ transition in the peptide bond of α -helical structure.⁴⁰ It was observed when treated with complex there is reduction in both of these bands without much shift of the peaks when treated with nickel complexes. The reduction is more in the case complex **1a** then **1b** indicating a more stronger influence on the disruption of helical structure of the protein for **1a**. However, when the complexes **1a** and **1b** was treated with HSA in 1:1 ratio the trend observed was something different. An increase in the percentage of α -helix formation was observed in both the cases with an increase in the intensity of negative band at 209 nm (fig S21). Though this phenomenon is relatively rare however there are some

examples where some metal complexes or other molecules when treated with proteins can increase the helicity of the α -helix with increase in its concentration.⁴¹ It has been envisaged that metal center may interact with carboxylate group present in the protein via coordinative interaction and simultaneously the ligand present in it can also exhibit hydrophobic interaction with the hydrophobic moieties in the protein chain. These two way interaction may have a cumulative effect of increase in percentage of α -helix component of HSA. These results indicated that the interaction between metal complexes with BSA and HSA may be not of similar nature however in the both cases the interaction causes a disruption in protein chain leading to the decrease of fluorescence intensities of the protein. The secondary structure composition of the peptide was estimated from CD spectra using K2D3 program⁴². All the results are tabulated and presented in table 4.

Catecholase activity study: To study the catecholase like activity of the synthesized metal complexes 3,5-di-tert-butylcatechol (3,5-DTBC) was taken as the substrate in the presence of two bulky t-butyl substituent in the ring it shows a low quinone-catechol reduction potential.⁴³ The reactions were carried out at 25°C in aerobic condition and it was monitored by UV-Vis spectroscopic technique (Scheme-S1). The oxidation product 3,5-di-tert-butylquinone (3,5-DTBQ) is highly stable and shows a maximum absorption at about 400 nm in methanol. To monitor the reaction a 10^{-4} M methanolic solution of different complexes (**1a** and **1b**) were treated with 100 equivalent of 3,5-BTDC in which upon addition of catecholic substrate a new band starts to gradually appear at about 402 nm with time due to the formation of the oxidized product 3,5-DTBQ (fig 4).

To understand the kinetic aspect of catalysis for **1a** and **1b**, the rate constant for a catalyst complex was determined by traditional initial rate method (detail description in experimental section). The observed rate versus substrate concentration data were then analyzed on the basis of the Michaelis–Menten approach of enzymatic kinetics. The Michaelis–Menten constant (K_M) and maximum initial rate (V_{max}) were determined by linearization using Lineweaver–Burk plots (fig S22).⁴⁴ The turnover number values (k_{cat}) were obtained by dividing the V_{max} values by the concentration of the corresponding complexes. All the data unambiguously demonstrate that both the complexes **1a** and **1b** are very much active. Complex **2a** did not respond to any kind of catalytic activity towards catechol oxidation as well. The unusual high activity of the mononuclear complex **1a** and **1b** may be attributed to the fact that the positive charge on the

piperazinyl moiety may help the facilitation of catalyst-substrate interaction by forming a positive channel which might be a prerequisite for showing better catalytic activities. A similar mechanism has been proposed to explain the activity of copper/zinc superoxide dismutase where positively charged arginine and lysine residue play a role to attract the anion and guiding them towards the catalytic center.²⁵

To draw probable mechanism (Scheme 2) of catecholase activity of **1a** (Comparatively higher K_{cat} value), we have investigated the probable complex-substrate intermediate through ESI-MS, change in d-d transition band of Ni(II) upon interaction with 3,5 DTBC through UV-Vis spectroscopy, and qualitative as well as quantitative detection of I_3^- band (~353nm.) by UV-Vis spectroscopy for indication of formation of H_2O_2 during catalytic oxidation procedure. ESI-MS positive spectrum of a 1:100 mixture of the proportionate complex **1a** and 3,5 DTBC, recorded after 5min of mixing exhibit two major peaks at $m/z = 243$ and 463 respectively, along with one small peak at 573.4 (fig S23A and S23B). The former two peaks correspond respectively to the quinone-sodium aggregates $[(3,5 DTBQ)Na]^+$ and $[(3,5 DTBQ)_2Na]^+$.⁴⁵ The later smaller peak at 573.4 could be due to the formation of complex-substrate aggregate (“C” / “D” in scheme-2) with a little deviation which is similar with earlier report.⁴⁶ Thus it is difficult to propose the exact structure of intermediate with the help of ESI-MS. Monitoring the catalytic reaction by UV-Vis spectroscopy reveals gradual formation of a very broad d-d transition bands (possibly combination of many bands) in the region of 650-900 nm (fig S24A and S24B). This result indicates the change of coordination environment of Ni(II) center from tetra coordinated to penta- or hexacoordinated.^{47,48} It is also important to note that, the dioxygen of atmosphere is reduced to H_2O_2 during the oxidation process. Oxidation of I^- to I_2 followed by the generation of I_3^- , qualitatively detected by UV-Vis spectral study of solution (fig S25), obtained after proper work up of the mixture of catechol, complex and KI, specifically indicates that dioxygen is reduced to H_2O_2 , as reported by earlier investigators²⁶. Quantitative analysis of H_2O_2 indicates that 0.8 mol (≈ 1) of H_2O_2 was shown to be produced per mol of 3,5 DTBC along with formation of 1 mol 3,5 DTBQ, which strongly supports the mechanism of reaction involving a two electron reduction process of areal oxygen, as indicated in previous reports⁴⁹. With the help of the all above experiments hereby it is proposed that the oxidation process is occurring in a radical pathway and possibly through a pentacoordinated intermediate as represented in scheme 2.

According to the reported generalized catecholase reaction mechanism²⁹ electron transfer is mainly facilitated by metal center and then further delocalized via C=N bond of metal Schiff-base complex to the adjacent conjugate system. In the present case the performance complex **1a** shows better catecholase activity than **1b** may due to the more delocalization of electrons along the conjugated aromatic ring via C=N in **1a**. All the obtained kinetic parameters are presented in table 5.

Conclusions :

In conclusion two new square planar nickel complexes $[\text{Ni}(\text{L}^1)]\text{ClO}_4$ **1a** and $[\text{Ni}(\text{L}^2)]\text{ClO}_4$ **1b** with Schiff base ligands L^1 and L^2 have been synthesized and characterized. Two more octahedral complexes were generated with combination of thiocyanate ion and L^1 and dmsu and L^2 , respectively where the Schiff-base ligand gets hydrolyzed and the resultant precursor amines takes up a chair conformation to act as bidentate ligand to furnish $[\text{Ni}(\text{SCN})_3(\text{CH}_3\text{OH})(\text{aminoethylpiperazineH})]$ **2a** and $[\text{Ni}(\text{DMSO})_4(\text{aminoethylpiperazineH})](\text{ClO}_4)_3$ **2b** where the secondary nitrogen atom in piperaziny ring remains protonated and staying away from coordination. All the complexes though primarily mononuclear in nature have shown complex hydrogen bonded network in three dimension. Complex **1a** showed strong interaction with DNA in both UV-visible absorption studies and competitive binding experiment in presence of ethidium bromide. The Scatchard plot gives a binding constant of $5.675 \times 10^3 \text{ M}^{-1}$ for compound **1a** and $2.340 \times 10^3 \text{ M}^{-1}$ for compound **1b**. The interaction of compound **1a** with albumin protein show intense interaction between metal complex and protein with very high fluorescence quenching. The Stern–Volmer quenching constant value obtained was to the tune of 10^{13} M^{-1} indicates that both static and dynamic quenching occurring simultaneously. The binding constant value obtained particularly for **1a**-HSA complex is exceptionally high and the number of binding site obtained was found to be almost equals to two. Moderate interaction is also detected between the complex **1b** and BSA and HSA with reasonable values of different kinetic parameters. This interaction gains further support from the data obtained from CD spectra of albumin proteins in presence of metal complexes **1a** and **1b**. Apart from the above mentioned interaction with biomolecules both the complexes **1a** and **1b** exhibited promising catecholase like activity with TON value to the order of 10^3 h^{-1} . Altogether this class of transition metal complexes have shown promising biological

activities and currently further studies are underway with similar class of ligands for future communications.

Experimental

Materials and Methods

All the chemical reagents required were purchased from sigma and used without further purification. Infrared spectra ($4000\text{--}500\text{cm}^{-1}$) were recorded with a BRUKER TENSOR 27 instrument in KBr pellets. NMR spectra was recorded in AVANCE III 400 Ascend Bruker BioSpin machine at ambient temperature. Mass spectrometric analyses had done on Bruker-Daltonics, microTOF-Q II mass spectrometer and elemental analyses were carried out with a ThermoFlash 2000 elemental analyzer. Spectrophotometric measurements were performed on a Varian UV-Vis spectrophotometer (Model: Cary 100) (for absorption) and Fluoromax-4p Spectrofluorometer from Horiba JobinYvon (Model: FM-100) (for emission) using a quartz cuvette with path length of 1 cm. Circular dichroism spectra were recorded by using a Jasco J-815 spectrometer (Jasco, Tokyo, Japan). Far-ultraviolet (UV) ($190\text{--}260\text{ nm}$) spectra were recorded in 0.1 cm path length cell (Hellma, Muellheim/Baden, Germany) using a step size of 0.5 nm, bandwidth of 1 nm and scan rate of 20 nm min^{-1} .

Caution! *Perchlorate compounds are potentially explosive. Only a small amount of material should be prepared and handled with care*

X-ray crystallography

Single crystal X-ray structural studies of **1a**, **1b**, **2a** and **2b** were performed on a CCD Agilent Technologies (Oxford Diffraction) SUPER NOVA diffractometer. Data for all the complexes were collected at 150(2) K for 1,2 and 3 using graphite-monochromated $\text{MoK}\alpha$ radiation ($\lambda_{\alpha} = 0.71073\text{ \AA}$). The strategy for the Data collection was evaluated by using the CrysAlisPro CCD software. The data were collected by the standard 'phi-omega scan techniques and were scaled and reduced using CrysAlisPro RED software. The structures were solved by direct methods using SHELXS-97 and refined by full matrix least-squares with SHELXL-97, refining on F^2 ⁵⁰.

The positions of all the atoms were obtained by direct methods. All non-hydrogen atoms were refined anisotropically. The remaining hydrogen atoms were placed in geometrically constrained positions and refined with isotropic temperature factors, generally $1.2 U_{eq}$ of their parent atoms. The crystal and refinement data are summarized in table 6. For complex **2a**, the C8 and C9 had been model for disorder.

Synthesis of 1-phenyl-3-((2-(piperidin-4-yl)ethyl)imino)but-1-en-1-ol (L¹) : 1.6218g (10 mmol) of Phenyl acetyl acetone dissolved in 10 mL of chloroform was added into a solution of 1.29g of amino ethyl piperazine (10 mmol) in 5 mL of chloroform. The mixture was stirred for 2 hours at room temperature. After evaporating the volatile solvent a yellow oily compound (L-1) is formed. Yield: 72%. ¹H NMR (400.13 MHz, 298 K, CDCl₃): δ 11.37 (s, 1H,-OH), 7.34-7.88 (m, 5H,aromatic H), 5.67 (s, 1H,vinyl H), 3.44 (q, 2H, cyclohexene -CH₂), 2.94 (t,4H, cyclohexene -CH₂), 2.61 (t, 2H, cyclohexene -CH₂), 2.51 (br t, 4H, aliphatic -CH₂), 1.88 (s, 4H,-CH₃ merged with -NH) ¹³C NMR (100.61 MHz, 293 K, DMSO): δ 187.8, 164.5, 140.5, 130.3, 128.1, 126.8, 92.3, 58.2, 54.4, 45.9, 40.5, 19.6.C₁₆H₂₃N₃O(m/z) calculated - 273.18 (m); obtained - 274.18 (m+H)⁺

Synthesis of 4-((2-(piperazin-1-yl)ethyl)imino)pent-2-en-2-ol (L²) : 1.00g (10 mmol) of Acetyl acetone dissolved in 10 mL of chloroform was added into a solution of 1.29 g of amino ethyl piperazine (10 mmol) in 5 mL of chloroform. The mixture was stirred for 2 hours at room temperature. After evaporating the volatile solvent a yellow oily compound (L-2) is formed. Yield: 72%. ¹H NMR (400.13 MHz, 298 K, CDCl₃): δ 10.78 (s, 1H, -OH), 4.94 (s, 1H, vinyl H), 3.33 (q, 2H, cyclohexene -CH₂), 2.89 (t, 4H, aliphatic -CH₂), 2.51 (t, 2H, cyclohexene -CH₂), 2.44 (br t, 4H, cyclohexene -CH₂), 1.97 (s, 4H, -CH₃ merged with -NH) 1.90 (s, 3H, -CH₃) ¹³C NMR (100.61 MHz, 293 K, CDCl₃): δ 194.3, 162.1, 94.8, 57.5, 53.9, 45.5, 39.7, 28.3, 18.6. C₁₁H₂₁N₃O (m/z) calculated - 211.16 (m); obtained - 212.17 (m+H)⁺.

Synthesis of [Ni(L¹)]ClO₄ (1a) : 15 mL of methanolic solution containing L¹ (0.13 g, 0.5mmol) and Ni(ClO₄)₂.6H₂O (0.182g, 0.5mmol) was stirred at room temp for 1hr and resulting red coloured solution was concentrated by evaporating the solvent. Finally after 2 or 3 days red needle shaped crystals were obtained from the reaction mixture after layering the mother liquor with diethyl ether. Yield: 85%. Anal.Calcd. (%) : C₁₆H₂₁ClN₃NiO₅ C, 44.74; H, 4.93; N, 9.78.

Found (%): C, 42.88; H, 5.13; N, 9.87. $[\text{C}_{16}\text{H}_{21}\text{N}_3\text{NiO}]^+$ (m/z) calculated – 330.05 (m)⁺; obtained – 330.10 (m)⁺. Selected IR on KBr (ν/cm^{-1}): 1597 (–C=N), 1097(ClO_4^-)

Synthesis of $[\text{Ni}(\text{L}^2)]\text{ClO}_4$ (1b) : 5 mL of methanolic solution containing L^2 (0.1055g, 0.5mmol) was added drop wise to a 10 mL solution of $\text{Ni}(\text{ClO}_4)_2 \cdot 6\text{H}_2\text{O}$ (0.182g, 0.5mmol) and the resultant mixture was stirred at room temp for 1hr and resulting red coloured solution was concentrated by evaporating the solvent. Layering of the reaction mixture with diethyl ether furnished red coloured needle shaped crystal after few days. Yield: 85%. Anal.Calcd. (%) : $\text{C}_{11}\text{H}_{19}\text{ClN}_3\text{NiO}_5$ C, 35.96; H, 5.21; N, 11.44. Found (%): C, 35.65; H, 5.43; N, 10.95. $[\text{C}_{11}\text{H}_{19}\text{N}_3\text{NiO}]^+$ (m/z) calculated – 267.98 (m)⁺; obtained – 268.19 (m)⁺. Selected IR on KBr (ν/cm^{-1}): 1605 (–C=N), 1105 (ClO_4^-) .

Synthesis of $[\text{Ni}(\text{SCN})_3(\text{CH}_3\text{OH})(\text{aminoethylpiperazineH})]$ (2a) : At first 15 ml of methanolic solution containing L^1 (0.1366g, 0.5mmol) and $\text{Ni}(\text{ClO}_4)_2 \cdot 6\text{H}_2\text{O}$ (0.182g, 0.5mmol) was stirred at room temp for 30 min. When the reaction mixture became red in colour, a 10 mL methanolic solution of NH_4SCN (0.076g, 1mmol) was added to it. The solution became green in colour and it was then concentrated by evaporating the solvent. Finally after 6 or 7 days green block shaped crystal of **2a** was obtained from reaction mixture after layering with diethyl ether. Yield: 55%. Anal.Calcd. (%) : $\text{C}_{10}\text{H}_{18}\text{N}_6\text{NiOS}_3$ C, 30.55; H, 4.61; N, 21.37. Found (%): C, 29.02; H, 4.85; N, 20.33. $[\text{C}_7\text{H}_{15}\text{N}_4\text{NiS}]^+$ (m/z) calculated – 245.03 (m)⁺; obtained – 245.05 (m)⁺. Selected IR on KBr (ν/cm^{-1}): 2092 (nitrogen bonded SCN).

Synthesis of $[\text{Ni}(\text{DMSO})_4(\text{aminoethylpiperazineH})](\text{ClO}_4)_3$ (2b) : 10ml aqueous solution containing L^2 (0.1055g, 0.5mmol) and $\text{Ni}(\text{ClO}_4)_2 \cdot 6\text{H}_2\text{O}$ (0.182g, 0.5mmol) was stirred at room temp for 1 hr and the resultant green solution was kept in the air for few days until the solvent evaporates to furnish a green powder. After that this dried green compound was dissolved in DMSO and layered by methanol for crystallisation. Green block shaped crystal of **2b** was obtained after one week time. Yield: 52%. Anal.Calcd. (%) : $\text{C}_{14}\text{H}_{39}\text{Cl}_3\text{N}_3\text{NiO}_{16}\text{S}_4$ C, 21.05; H, 4.92; N, 5.26. Found (%): C, 19.99; H, 5.07; N, 5.52. $[\text{C}_8\text{H}_{21}\text{N}_3\text{NiOS}]^{3+}$ (m/z) calculated – 265.07 (m+); obtained – 282.27 (m+ H_2O).

DNA Binding Study : All the experiments concerning the interaction of the complexes with calf thymus (CT) DNA were performed in Tris–HCl buffer (50 mMTris–HCl, pH 7.4). A buffer

solution of CT DNA gave a ratio of UV absorbance at 260 and 280 nm of about 1.8:1, specifying the CT DNA sufficiently free from protein. The DNA concentration was measured by its extinction coefficient at 260 nm ($6600 \text{ M}^{-1} \text{ cm}^{-1}$) after 1:100 dilution. Stock solutions were stored at 4 °C and used not more than 4 days. Absorption titration was done by keeping fixed metal complex concentration at 10 μM while changing the CT-DNA conc. from 0 to 200 μM . During titration equal quantity of CT-DNA was added to both complex solution and reference solution to eliminate the absorbance of CT-DNA itself. Furthermore DNA binding for complexes (**1a** and **1b**) is measured by a special fluorescence spectral technique; ETBr displacement assay from ETBr bound CT-DNA in Tris-HCl buffer at biological pH 7.4. The changes in fluorescence intensities at 605 nm (520 nm excitation) of EB (20 μM) bound to DNA were measured with respect to concentration of the complex (0-100 μM). EB was non-emissive in Tris-HCl buffer solution (pH 7.4) due to fluorescence quenching of the free EB by the solvent molecules.

Protein Binding Study : The binding interactions experiments of complexes **1a** and **1b** with BSA and HSA protein were carried out using standard Trp fluorescence with excitation at 295 nm and the corresponding emission at 340 nm, using a Fluoromax-4p Spectrofluorometer [from Horiba JobinYvon (Model: FM-100)] with a rectangular quartz cuvette of 1 cm path length. A stock solution of BSA and HSA protein were prepared in TRIS-HCl buffer (pH ~7.4). Concentrated stock solutions of complexes **1a** and **1b** were prepared by dissolving them separately in TRIS-HCl buffer and diluted suitably with TRIS-HCl buffer to get the required concentrations. An aqueous solution (2 mL) of BSA or HSA protein (10 μM) was titrated by successive additions of the respective complexes (0-100 μM). Interaction with proteins is also monitored by measuring increment of absorption band at 278nm in UV-Vis spectroscopy through successive addition of 0-100 μM of **1a** and **1b** in 10 μM protein solution.

Circular dichroism measurements : Four successive scans recorded at a scan speed of 50 nm^{-1} were averaged out to obtain the CD spectra of serum albumins. Appropriate blank (tris buffer) was subtracted to attain the final result. Monitoring the far UV-CD spectra (200-250 nm) provides important information to get insight about the change in secondary structure of serum albumin proteins. At first the spectra of free BSA (10 μM) and HSA (10 μM) was recorded and then changes in CD spectra were obtained by monitoring the binding of metal complexes upon addition of 20 μM of metal complexes successively.

Catecholase activity study :100 equivalent of 3,5-di-tertbutylcatechol (3,5-DTBC) in methanol were added to 10^{-4} M solutions of **1a**, **1b**, and **2a** in methanol under aerobic condition. Absorbance of the resultant reaction mixture was plotted with respect to wavelength at a regular interval of 10 min in a spectrophotometer in the range of 300-500 nm. The dependence of the rate on various concentration and different kinetic parameters were obtained by treatment of a 10^{-4} M solution of different complexes with 20 to 500 equivalent of substrate and monitoring the upsurge in absorbance at 402 nm (the peak corresponding to the quinone band maxima) as a function of time.

Note :*Due poor solubility of 2b in MeOH and Aq. Buffer, the catecholase study and protein binding study were not performed.*

Detection of Hydrogen Peroxide in the Catalytic Reactions

Modification of iodometric method is employed to detect H_2O_2 quantitatively during the catalytic reaction. Reaction mixtures were prepared as in the kinetic experiments. After 1 h of reaction an equal volume of water was added to extract the formed quinone using dichloromethane. The aqueous layer was acidified with H_2SO_4 to $\text{pH} \approx 2$ to stop further oxidation, and 1 mL of a 10% solution of KI and three drops of 3% solution of ammonium molybdate were added. In the presence of hydrogen peroxide I^- is oxidised to I_2 , $\text{H}_2\text{O}_2 + 2\text{I}^- + 2\text{H}^+ \rightarrow 2\text{H}_2\text{O} + \text{I}_2$, and with an excess of iodide ions, the tri-iodide ion is formed according to the reaction $\text{I}_2(\text{aq}) + \text{I}^- \rightarrow \text{I}_3^-$. The reaction rate is slow but increases with increasing concentrations of acid, and the addition of an ammonium molybdate solution condenses the reaction almost immediate. The formation of I_3^- could be monitored by UV-vis spectroscopy due to the development of the characteristic I_3^- band ($\lambda = 353 \text{ nm}$, $\epsilon = 26\,000 \text{ M}^{-1} \text{ cm}^{-1}$).

Detection of d-d transition band in the Catalytic Reactions

Time dependent UV-Vis spectra was recorded in the range 500-1100 nm after mixing of complex with 3,5 DTBC. Formation of new band (d-d transition band) near 700-800nm indicates that coordination of Ni(II) changes from 4 to 5 or 6 during formation of complex-substrate aggregate.

Supplementary Materials

CCDC 995060,995058, 995061 and 995059 contain the supplementary crystallographic data for **1a**, **1b**, **2a** and **2b**, respectively. These data can be obtained free of charge via <http://www.ccdc.cam.ac.uk/conts/retrieving.html>, or from the Cambridge Crystallographic Data Centre, 12 Union Road, Cambridge CB2 1EZ, UK; fax: (+44) 1223-336-033; or e-mail: deposit@ccdc.cam.ac.uk.

Acknowledgement

We are thankful to Sophisticated Instrument Centre, IIT Indore for the structure elucidation. The authors acknowledge Surajit Chatterjee, Arpan Bhattacharya and Anupam Das for unimpeachable help in bio-physical part of this work. We are also thankful to the referees for suggesting to perform many other experiments to considerably improve the quality of the work presented here.

References:

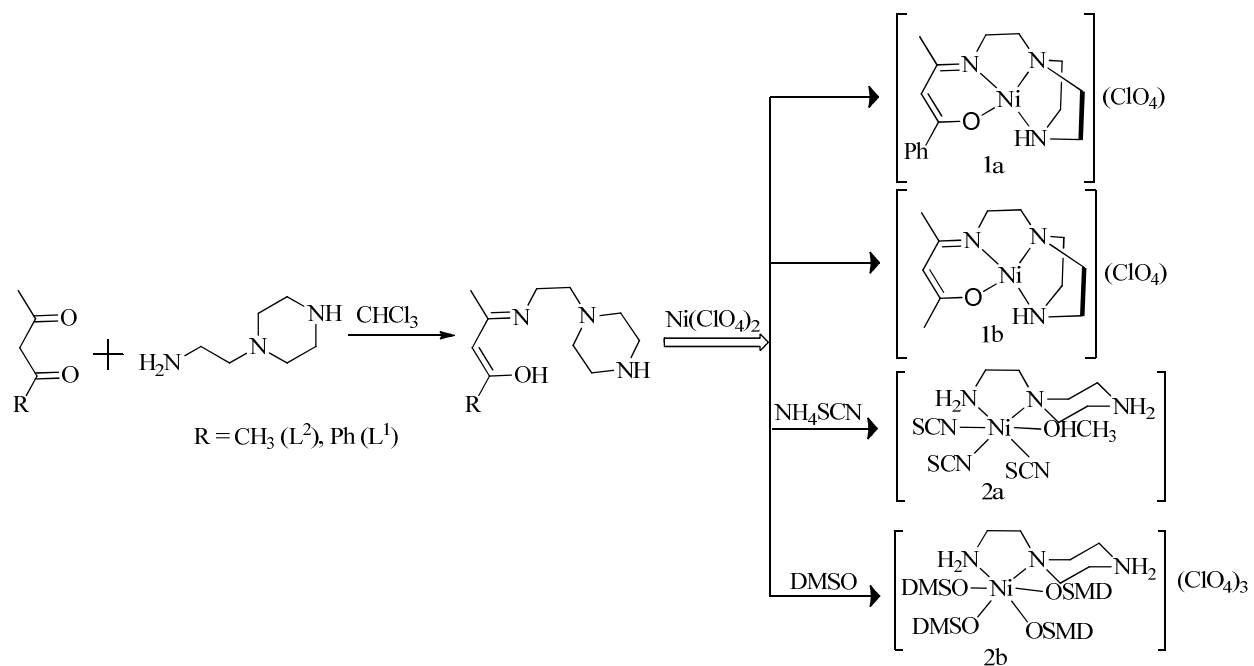
1. D. Tietze, M. Tischler, S. Voigt, D. Imhof, O. Ohlenschläger, M. Görlach and G. Buntkowsky, *Chemistry – A European Journal*, 2010, **16**, 7572-7578.
2. S. M. Barnett, Goldberg, K. I., Mayer, J. M., *Nat. Chem.*, 2012, **4**, 498.
3. S. Shaik, *Nat Chem*, 2010, **2**, 347-349.
4. A. Mukherjee, *Biomimetics Learning from Nature*, InTech, **2010**.
5. D. M. L. D. Bethany N. Wigington, Prof. Dr. Thomas R. Cundari, Dr. David L. Thorn, Dr. Susan K. Hanson³, and Prof. Dr. Susannah L. Scott, *Chemistry - A European Journal*, 2012, **18**, 14981-14988.
6. B. Meunier, *Biomimetic oxidations catalyzed by transition metal complexes*, Imperial college press: **2000**.
7. C. T. S. Zahid H. Chohan , Andrea Scozzafava, *J Enzym Inhibition and Med. Chem.*, 2004, **19**, 79-84.

8. R. del Campo, J. J. Criado, E. García, M. a. R. Hermosa, A. Jiménez-Sánchez, J. L. Manzano, E. Monte, E. Rodríguez-Fernández and F. Sanz, *Journal of Inorganic Biochemistry*, 2002, **89**, 74-82.
9. N. C. Kasuga, K. Sekino, C. Koumo, N. Shimada, M. Ishikawa and K. Nomiya, *Journal of Inorganic Biochemistry*, 2001, **84**, 55-65.
10. P. C. A. Bruijninx, P. J. Sadler, *Current Opinion in Chemical Biology* 2008, **12**, 197.
11. A. Vessieres, S. Top, W. Beck, E. Hillard and G. Jaouen, *Dalton Transactions*, 2006, DOI: 10.1039/B509984F, 529-541.
12. L. J. K. Boerner, J. M. Zaleski, *Current Opinion in Chemical Biology* 2005, **9**, 135.
13. V. C. Silveira, M. P. Abbott, M. Cavicchioli, M. B. Goncalves, H. M. Petrilli, L. de Rezende, A. T. Amaral, D. E. P. Fonseca, G. F. Caramori and A. M. da Costa Ferreira, *Dalton Transactions*, 2013, **42**, 6386-6396.
14. A. Patra, T. K. Sen, A. Ghorai, G. T. Musie, S. K. Mandal, U. Ghosh and M. Bera, *Inorganic Chemistry*, 2013, **52**, 2880-2890.
15. X.-W. Li, L. Tao, Y.-T. Li, Z.-Y. Wu and C.-W. Yan, *European Journal of Medicinal Chemistry*, 2012, **54**, 697-708.
16. P. Kalaivani, S. Saranya, P. Poornima, R. Prabhakaran, F. Dallemer, V. Vijaya Padma and K. Natarajan, *European Journal of Medicinal Chemistry*, 2014, **82**, 584-599.
17. A. Lauria, R. Bonsignore, A. Terenzi, A. Spinello, F. Giannici, A. Longo, A. M. Almerico and G. Barone, *Dalton Transactions*, 2014, **43**, 6108-6119.
18. W. Bal, J. Lukszo and K. S. Kasprzak, *Chemical Research in Toxicology*, 1997, **10**, 915-921.
19. P. li, M. Niu, M. Hong, S. Cheng and J. Dou, *Journal of Inorganic Biochemistry*, 2014, **137**, 101-108.
20. F. Le, D. Sun, D. Liu, C. Zheng, Y. Liu and J. Liu, *Inorganic Chemistry Communications*, 2013, **38**, 20-27.
21. P. Krishnamoorthy, P. Sathyadevi, R. R. Butorac, A. H. Cowley, N. S. P. Bhuvanesh and N. Dharmaraj, *Dalton Transactions*, 2012, **41**, 6842-6854.
22. E. Ramachandran, D. S. Raja, J. L. Mike, T. R. Wagner, M. Zeller and K. Natarajan, *RSC Advances*, 2012, **2**, 8515-8525.

23. P. Krishnamoorthy, P. Sathyadevi, R. R. Butorac, A. H. Cowley, N. S. P. Bhuvanesh and N. Dharmaraj, *Dalton Transactions*, 2012, **41**, 4423-4436.
24. A. Basu, D. Thiyagarajan, C. Kar, A. Ramesh and G. Das, *RSC Advances*, 2013, **3**, 14088-14098.
25. T. Chattopadhyay, M. Mukherjee, A. Mondal, P. Maiti, A. Banerjee, K. S. Banu, S. Bhattacharya, B. Roy, D. J. Chattopadhyay, T. K. Mondal, M. Nethaji, E. Zangrando and D. Das, *Inorganic Chemistry*, 2010, **49**, 3121-3129.
26. A. Biswas, L. K. Das, M. G. B. Drew, G. Aromí, P. Gamez and A. Ghosh, *Inorganic Chemistry*, 2012, **51**, 7993-8001.
27. L. K. Das, A. Biswas, J. S. Kinyon, N. S. Dalal, H. Zhou and A. Ghosh, *Inorganic Chemistry*, 2013, **52**, 11744-11757.
28. T. Ghosh, J. Adhikary, P. Chakraborty, P. K. Sukul, M. S. Jana, T. K. Mondal, E. Zangrando and D. Das, *Dalton Transactions*, 2014, **43**, 841-852.
29. Adhikary, P. Chakraborty, S. Das, T. Chattopadhyay, A. Bauzá, S. K. Chattopadhyay, B. Ghosh, F. A. Mautner, A. Frontera and D. Das, *Inorganic Chemistry*, 2013, **52**, 13442-13452.
30. A. Guha, K. S. Banu, S. Das, T. Chattopadhyay, R. Sanyal, E. Zangrando and D. Das, *Polyhedron*, 2013, **52**, 669-678.
31. Faulkner; R. Webster, Rostek; Jr. J. Charles, *Eur. Pat. Appl.*1990, EP 399986 A1 19901128.
32. (a) S. Naiya, B. Sarkar, Y. Song, S. Ianelli, M. G. B. Drew, A. Ghosh, *Inorg. Chim. Acta*2010, **363**, 2488–2495. (b) P. Mukherjee, M. G. B. Drew, A. Ghosh, *Eur. J. Inorg. Chem.*2008, 3372–3381. (c) C. Biswas, S. Chattopadhyay, M. G. B. Drew, A. Ghosh, *Polyhedron*2007, **26**, 4411–4418. (d) M.F. Mahon *et al.* *Inorg. Chim. Acta.*2009, **362**, 2353–2360.
33. S. Mukhopadhyay, D. Mandal, D. Ghosh, I. Goldberg and M. Chaudhury, *Inorganic Chemistry*, 2003, **42**, 8439-8445.
34. K. Nakamoto, *Infrared and Raman Spectra of Inorganic and Coordination Compounds, Theory and Applications in Inorganic Chemistry*, John Wiley & Sons, Inc.: Hoboken, New Jersey, 6th edn, 2009.
35. G. A. Garwood, R.A. Condrate, *Clays and Clay Minerals*, 1978, **26**, 273-278.

36. P. Krishnamoorthy, P. Sathyadevi, A. H. Cowley, R. R. Butorac and N. Dharmaraj, *European Journal of Medicinal Chemistry*, 2011, **46**, 3376-3387.
37. S. Lin *et al.* *Bioorg. Med. Chem. Lett.* 2010, **20**, 5864–5868.
38. X.-W. Li, X.-J. Li, Y.-T. Li, Z.-Y. Wu and C.-W. Yan, *Journal of Photochemistry and Photobiology B: Biology*, 2013, **118**, 22-32.
39. A. Ray, B. Koley Seth, U. Pal and S. Basu, *Spectrochimica Acta Part A: Molecular and Biomolecular Spectroscopy*, 2012, **92**, 164-174.
40. D. Li, M. Zhu, C. Xu and B. Ji, *European Journal of Medicinal Chemistry*, 2011, **46**, 588-599.
41. (a) N. S. Raja, H. Y. Srivastava, B. U. Nair, *Indian Journal of Chemistry*, 2011, **50A**, 531-538. (b) T. Chatterjee, A. Pal, S. Dey, B. K. Chatterjee, P. Chakrabarti, *PLOS ONE* 2012, **7**, e37468. (c) A. Barzegar, Ali. A. Moosavi-Movahedi, N. Sattarahmady, Md. A. Hosseinpour-Faizi, Md. Aminbakhsh, F. Ahmad, Ali. A. Saboury, Md. R. Ganjali, P. Norouzi, *Protein & Peptide Letters* **2007**, **14**, 13-18.
42. C. Louis-Jeune, M. A. Andrade-Navarro, C. Perez-Iratxeta, Prediction of Protein Secondary Structure from Circular Dichroism Using Theoretically Derived Spectra. *Proteins* 2012, **80**, 374–381.
43. S. K. Dey and A. Mukherjee, *ChemCatChem*, 2013, **5**, 3533-3537.
44. A. Jana, N. Aliaga-Alcalde, E. Ruiz and S. Mohanta, *Inorganic Chemistry*, 2013, **52**, 7732-7746.
45. S. Sarkar, S. Majumder, S. Sasmal, L. Carrella, E. Rentschler, S. Mohanta, *Polyhedron*, 2013, **50**, 270–282
46. K. S. Banu, T. Chattopadhyay, A. Banerjee, S. Bhattacharya, E. Suresh, M. Nethaji, E. Zangrando, and D. Das, *Inorganic Chemistry*, 2008, **47**, 7083-7093.
47. D. N. Sathyanarayana, *Electronic Absorption Spectroscopy and Related Techniques*, Universities press (India) Limited, **2001**.
48. D. Gatteschi and A. Scozzafava, *Inorganica Chimica Acta*, 1977, **21**, 223-227.
49. R. Marion, G. Muthusamy and F. Geneste, *Journal of Catalysis*, 2012, **286**, 266-272.
50. G. Sheldrick, *Acta Crystallographica Section A*, 2008, **64**, 112-122.

Schemes :



Scheme 1 : Formation of metal complexes with boat and chair conformer of piperazine moiety.

Figures :

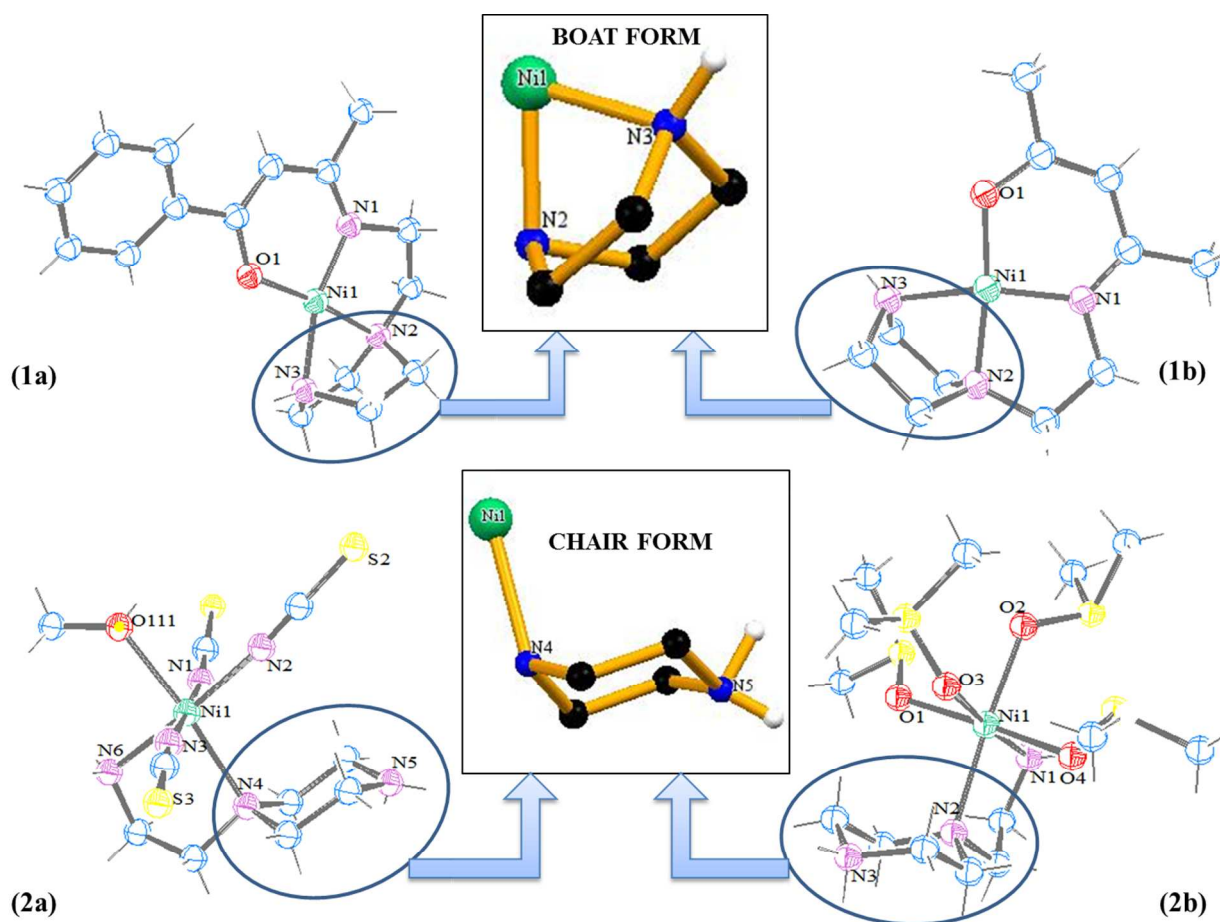


Fig 1: Different coordination environment of complexes (1a, 1b, 2a and 2b) (All non-coordinated ClO_4^- ions are hidden for clarity). Boat and Chair conformation of piperazine moiety (Inset).

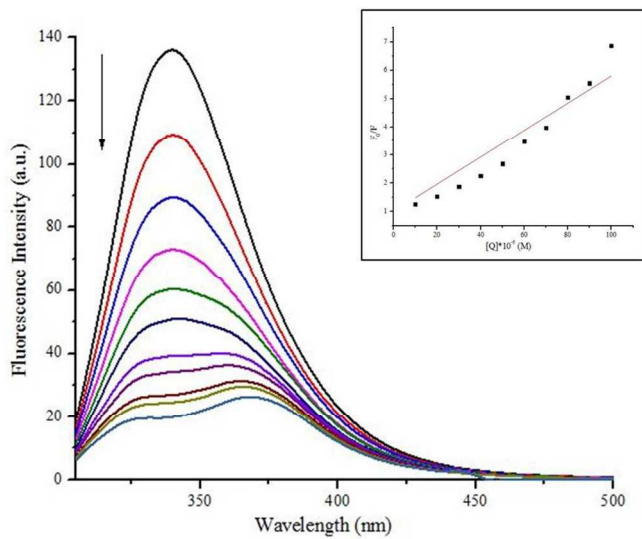


Fig 2: Fluorescence quenching of BSA by **1a**. Stern-Volmer plot is in Inset.

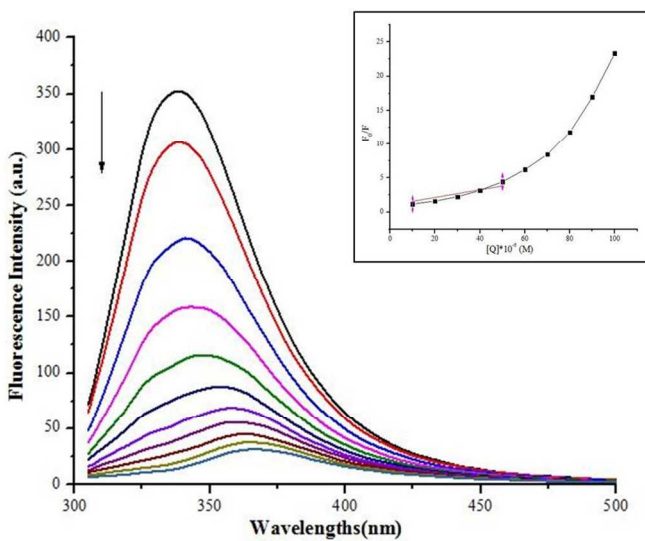


Fig 3: Fluorescence quenching of HSA by **1a**. Stern-Volmer plot is in Inset.

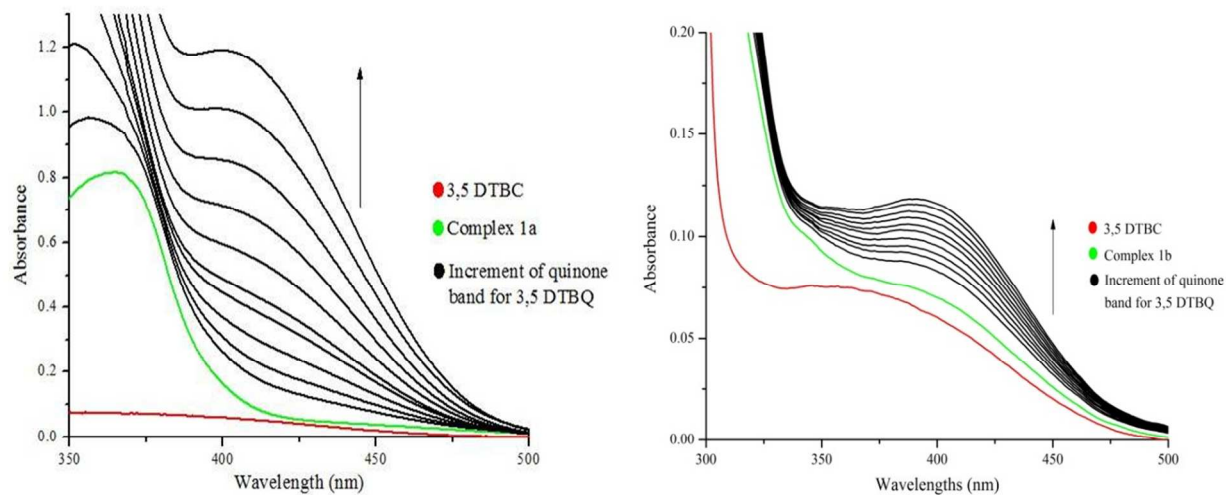


Fig 4: Showing catecholase activity by change in time dependent spectral pattern of complex **1a**(left) and **1b** (right) after addition of 3,5 DTBC.

Tables :

Table 1 :Selected bond lengths (\AA) and bond angles ($^\circ$) for **1a** and **1b**.

Complex	1a	1b
Ni(1)-O(1)	1.8112(17)	1.814(2)
Ni(1)-N(1)	1.830(2)	1.832(3)
Ni(1)-N(2)	1.883(2)	1.883(3)
Ni(1)-N(3)	1.934(2)	1.928(3)
O(1)-Ni(1)-N(1)	98.07(9)	98.14(12)
N(1)-Ni(1)-N(2)	88.56(11)	89.20(12)
O(1)-Ni(1)-N(3)	96.92(9)	96.95(12)
N(2)-Ni(1)-N(3)	76.58(10)	76.01(12)

Table 2 :Selected bond lengths (Å) and bond angles (°) for **2a** and **2b**.

2a		2b	
Ni(1)-N(2)	2.042(2)	Ni(1)-O(4)	2.045(3)
Ni(1)-N(3)	2.059(2)	Ni(1)-O(1)	2.052(3)
Ni(1)-N(6)	2.061(2)	Ni(1)-N(1)	2.084(4)
Ni(1)-N(1)	2.070(3)	Ni(1)-O(3)	2.093(3)
Ni(1)-O(111)	2.165(2)	Ni(1)-O(2)	2.110(3)
Ni(1)-N(4)	2.257(2)	Ni(1)-N(2)	2.238(3)
N(2)-Ni(1)-N(3)	90.22(10)	O(4)-Ni(1)-N(1)	89.35(14)
N(3)-Ni(1)-N(6)	90.12(11)	O(1)-Ni(1)-N(1)	94.33(14)
N(2)-Ni(1)-N(1)	89.12(10)	O(4)-Ni(1)-O(3)	87.92(11)
N(6)-Ni(1)-N(1)	90.38(11)	O(1)-Ni(1)-O(3)	88.53(12)
N(2)-Ni(1)-O(111)	85.40(10)	O(4)-Ni(1)-O(2)	93.70(12)
N(3)-Ni(1)-O(111)	90.98(9)	O(1)-Ni(1)-O(2)	89.41(12)
N(6)-Ni(1)-O(111)	91.01(9)	N(1)-Ni(1)-O(2)	91.51(14)
N(1)-Ni(1)-O(111)	86.35(10)	O(3)-Ni(1)-O(2)	86.17(12)
N(2)-Ni(1)-N(4)	101.00(9)	O(4)-Ni(1)-N(2)	85.09(13)
N(3)-Ni(1)-N(4)	90.33(10)	O(1)-Ni(1)-N(2)	92.20(13)
N(6)-Ni(1)-N(4)	82.59(10)	N(1)-Ni(1)-N(2)	82.61(15)
N(1)-Ni(1)-N(4)	92.38(10)	O(3)-Ni(1)-N(2)	99.64(12)

Table 3 :Table for Stern-Volmer quenching const. , binding const., binding site.

System	K_{SV} (M⁻¹)	K_q (M⁻¹S⁻¹)	K_a (M⁻¹)	n
1a -BSA --	4.8x10 ⁴	7.7x10 ¹²	1.7x10 ⁶	1.34
1b -BSA --	2.7x10 ³	4.3x10 ¹¹	4.9x10 ³	1.07
1a -HSA --	1.4x10 ⁵	2.2x10 ¹³	5.6x10 ⁹	2.12
1b -HSA --	3.1x10 ³	5.0x10 ¹¹	5.1x10 ³	1.03

Table 4 :Table for CD measurement analysis.

System	α -Helix %	β -Sheet %
Free BSA	68.87	9.59
BSA-1a	68.33	9.72
BSA-1b	68.55	9.64
Free HSA	67.88	9.85
HSA-1a	68.38	9.79
HSA-1b	68.34	9.81

Table 5 :Table for various kinetic parameter of catecholase activity.

Complex /Catalyst	Fixed Complex/Catalyst Conc. (M)	V_{\max} (M min ⁻¹)	Std. Error	K_M (M)	Std. Error	K_{cat} / T.O.N (h ⁻¹)
1a	0.0002	0.02671	3.4X10 ⁻⁴	0.08335	0.00283	8.0X10 ³
1b	0.0001	0.00455	2.8X10 ⁻⁴	0.00158	3.7X10 ⁻⁴	2.7X10 ³

Table 6 :Crystallographic data and structure refinement parameters for **1a**, **1b**, **2a** and **2b**.

Complex	1a	1b	2a	2b
Empirical Formula	C ₁₆ H ₂₁ ClN ₃ NiO ₅	C ₁₁ H ₂₀ ClN ₃ NiO ₅	C ₁₀ H ₁₉ N ₆ NiO ₅ S ₃	C ₁₄ H ₃₉ Cl ₃ N ₃ NiO ₁₆ S ₄
Formula weight	429.52	368.46	394.19	798.78
Crystal system	Orthorhombic	Orthorhombic	Orthorhombic	Monoclinic
Space group	P b c a	P 21 21 21	P c a 21	P 21
a (Å)	10.1342(2)	7.6658(3)	15.8598(3)	10.2345(2)
b (Å)	17.1147(3)	10.5251(6)	9.9515(2)	11.2429(2)
c (Å)	21.5781(4)	18.7540(6)	10.9722(2)	14.6064(2)
α (°)	90	90	90	90

β (°)	90	90	90	94.1040(10)
γ (°)	90	90	90	90
V (Å ³)	3742.59(12)	1513.13(12)	1731.73(6)	1676.38(5)
λ (Å)	1.5418	0.71073	0.71073	0.71073
ρ_{calcd} (mg m ⁻³)	1.525	1.617	1.512	1.582
Z	8	4	4	2
T (K)	150(2)	150(2)	150(2)	150(2)
μ (mm ⁻¹)	3.098	1.483	1.488	1.133
F(0 0 0)	1784	768	820	830
Crystal size (mm ³)	0.33 x 0.26 x 0.21	0.33 x 0.26 x 0.21	0.33 x 0.26 x 0.21	0.23 x 0.17 x 0.14
θ ranges (°)	4.10 - 72.18	3.29 - 25.00	3.05 - 24.99	2.97 - 25.00
h/k/l	-9,12/-20,21/-25,26	-9,7/-11,12/-20,22	-18,18/-11,11/-13,13	-12,11/-13,12/-17,17
Reflections collected	26518	10881	12554	13277
Independent reflections	3684	2656	3023	4893
T _{max} and T _{min}	0.5624 and 0.4280	0.7460 and 0.6404	0.7452 and 0.6394	0.8575 and 0.7806
Data/restraints/parameters	3684 / 0 / 273	2656 / 0 / 194	3023 / 1 / 203	4893 / 1 / 390
Goodness-of-fit (GOF) on F ²	1.063	1.087	1.051	1.051
Final R indices [I > 2 σ (I)]	R1 = 0.0469, wR2 = 0.1400	R1 = 0.0302, wR2 = 0.0784	R1 = 0.0292, wR2 = 0.0749	R1 = 0.0363, wR2 = 0.0975
R indices (all data)	R1 = 0.0546, wR2 = 0.1490	R1 = 0.0338, wR2 = 0.0815	R1 = 0.0302, wR2 = 0.0761	R1 = 0.0383, wR2 = 0.0998
Largest peak and hole (e Å ⁻³)	0.477 and -0.365	0.385 and -0.218	0.428 and -0.454	0.484 and -0.299

Table of Contents Graphic

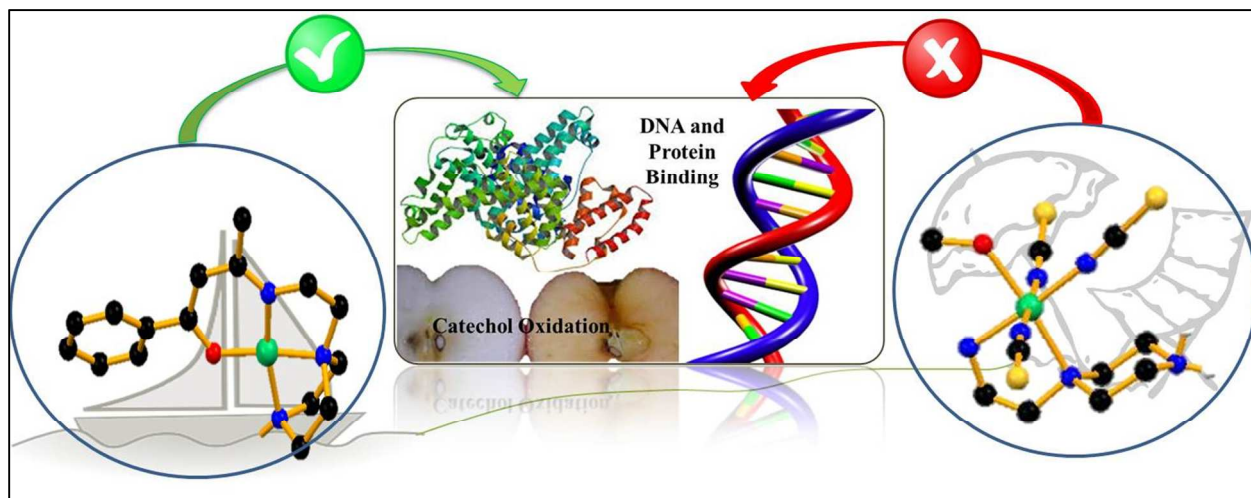


Table of Contents Graphic

Nickel complexes with flexible piperazinyl moiety are showing interesting DNA and protein binding properties and catecholase like activity in boat conformation.

